A novel absorption thermal storage system dynamic model for thermal energy storage[#]

Zhenpeng Deng, Shuo Wang, Hua Chen, Wen-long Cheng*

Department of Thermal Science and Energy Engineering, University of Science and Technology of China, Hefei, Anhui 230027, China
(Wen-Long Cheng: wlcheng@ustc.edu.cn)

ABSTRACT

Thermal energy storage plays an important role in renewable energy utilization. Absorption thermal storage （ATS） is used to balance heat source and load due to its high stability. To investigate the charging and discharging process of ATS, a novel dynamic ATS model was proposed and validated. Based on the established model, the effects of charging temperature, discharging temperature, condenser inlet temperature, and evaporator inlet temperature on the performance of thermal storage were analyzed. The results show that the higher charging temperature increases solution glide, resulting in improved energy storage efficiency and energy storage density. The maximum energy storage efficiency is between 0.25 and 0.65, while the maximum energy storage density varies from 55.6 kWh/m^3 to 143.6 kWh/m^3, with discharging temperatures of 70–90 °C. Increasing the condenser inlet temperature and decreasing the evaporator inlet temperature significantly reduces the charging time and discharging time, respectively.

Keywords: absorption thermal storage, energy storage efficiency, energy storage density

NONMENCLATURE

Abbreviations	
ATS	Absorption thermal storage
ESE	Energy storage efficiency
ESD	Energy storage density
Symbols	
A	heat transfer area, m^2
C_p	specific heat, kJ/(kg·°C)
h	enthalpy, kJ/kg
M	mass, kg
Pr	Prandtl number
Q	thermal energy, kW
Re	Reynolds number
t	time, s
T	temperature, °C

U	overall heat transfer coefficient, W/(m^2·°C)
A	heat transfer area, m^2
V	volume, m^3
Γ	mass flow rate per unit length, kg/(m·s)
W	energy consumption, kW
X	solution concentration
α	heat transfer coefficient, kW/(m^2·°C)
v	kinematic viscosity, m^2/s
η	efficiency
ρ	density, kg/m^3
λ	thermal conductivity, kW/(m·°C)
δ	thickness, m
Subscripts	
p	pump
r	refrigerant
s	solution
v	vapor refrigerant

1. INTRODUCTION

Thermal energy storage technology is widely used in renewable energy applications to balance energy consumption and supply [1]. Absorption thermal storage (ATS) provides higher energy density by storing thermal energy as chemical energy. It contributes to prolonged energy storage and easier transportation over long distances [2]. The ATS has a variety of energy storage and release for dehumidification, cooling or heating [3].

In recent years, the growth of ATS research has focused on the charging and discharging process and improving energy storage density (ESD) and energy storage efficiency (ESE). Many scholars have conducted experimental or numerical studies on the characteristics of ATS [4]. Zhang et al. [5] designed and built an ATS experimental plant with 10 kWh cooling storage capacity. The ESE for cooling, domestic hot water and heating of the ATS system are 0.51, 0.97 and 1.03, respectively. Ding et al. [6] developed a hybrid double-

---

effect compression-assisted ATS system, adding a compressor improves system performance. Liu et al. [7] built a refrigeration model coupled with an ATS system, and the results show that the total refrigerating capacity and average performance coefficient increased by 4.44% and 3.5%. Wen et al. [8] proposed a six-order dynamic nonlinear state-space model of a single-effect absorption chiller considering dynamic processes in subcomponents. Results of both steady and dynamic comparisons prove good correctness of the proposed model. However, there is a lack of research on the dynamic characteristics of the charging and discharging process. The current model has a large error in the pre-operational process. Therefore, it is necessary to establish a dynamic model of absorption energy storage to study the dynamic performance during the charging and discharging process.

In this paper, based on the conventional single-stage LiBr ATS model, a new dynamic ATS model was first developed by transiently correcting the vapor mass flow rate. Then, based on the established model, the energy storage characteristics of charging temperature and discharging temperature are analyzed. Finally, the effects of different condenser inlet temperatures and evaporator inlet temperatures on the charging and discharging times are investigated.

2. SYSTEM DESCRIPTION

Fig. 1 shows an absorption thermal energy storage system including a solution tank, a refrigerant tank, two heat exchangers and valves. The heat exchanger is installed inside the tank. H_2O/LiBr is used as the working fluid in this investigation.

During the charging process, thermal energy is transferred to the solution tank through the heat exchanger, resulting in a vapor pressure difference between the solution tank and the refrigerant tank. The vapor evaporates from the solution tank into the refrigerant tank. The solution is increasingly concentrated to charge the thermal energy.
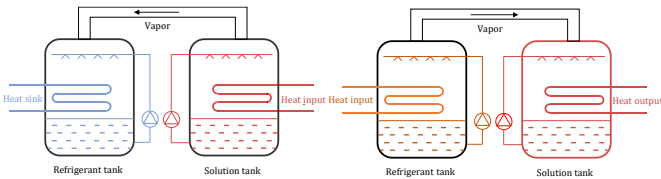

Fig.1 Schematic diagram of absorption thermal energy storage system (a) charging process, (b) discharging process.

During the discharging process, low temperature thermal energy is transferred to the refrigerant tank through the heat exchanger. Vapors flow from the refrigerant tank to the concentrated solution tank with the absorption heat released. The solution is increasingly decreased to discharge high-grade energy.

3. THE ABSORPTION ENERGY STORAGE DYNAMIC MODEL

3.1 Simplifying assumptions

To facilitate the dynamic modelling of absorption energy storage systems, the following assumptions are required to be made:

1. The temperature, pressure and mass concentration are homogeneous in the solution and refrigerant components.

2. The thermal storage of the shell and tube of the exchanger is neglected.

3. The heat loss between the shell and the environment is neglected.

4. The cooling/heating water has no mass/energy accumulation, and its thermal properties keep constant.

5. The solution pump is isentropic, and the heat input by the pump is neglected.

3.2 General balance equations of the model

In the charging process, the refrigerant in the solution tank is heated and evaporated to flow into the refrigerant tank. And in the discharging process, the refrigerant vapor is condensed and releases heat in solution tanks. Absorption heat storage system depends on the latent heat of the refrigerant to store/release thermal energy. The overall mass conservation equation during the charging/discharging process is as follows:

$$\frac{dM_s(t)}{dt} = -\dot{m}_v(t) \tag{1}$$

where M_s is the solution mass, t is the running time, $\dot{m}_v$ is the mass flow rate of refrigerant vapor. The positive $\dot{m}_v$ represents that the flow direction is from the solution tank to the refrigerant tank and the negative represents that the flow direction is from the refrigerant tank to the solution tank.

The mass conservation equation of LiBr during the charging/discharging process is as follows:

$$\frac{d[M_s(t) \cdot X(t)]}{dt} = 0 \tag{2}$$

where $X(t)$ is the concentration of the solution.

The energy conservation equation for the Libr solution in the generator/absorber is as follows:

$$\frac{d[M_s(t) \cdot h_s(t)]}{dt} = -\dot{m}_v(t) \cdot h_v(t) + Q_s(t) \tag{3}$$

where $h_s(t)$ is the specific enthalpy of the solution, $h_v(t)$ is the specific enthalpy of the refrigerant vapor, $Q_s(t)$ is the heat transfer rate between solution and water.

The energy conservation equation for the refrigerant in the condenser/evaporator is as follows:

$$\frac{d[M_r(t) \cdot h_r(t)]}{dt} = \dot{m}_v(t) \cdot h_v(t) - Q_r(t) \qquad (4)$$

where $h_r(t)$ is the specific enthalpy of the refrigerant. $Q_r(t)$ is the heat transfer rate between refrigerant and water.

Inserting Eq. (1) into Eq. (2) reads:

$$\frac{dX(t)}{dt} = \frac{X(t) \cdot \dot{m}_v(t)}{M_s(t)} \qquad (5)$$

Inserting Eq. (1) into Eq. (3) reads:

$$\frac{dT_s(t)}{dt} = \frac{(h_s(t) - h_v(t)) \cdot \dot{m}_v(t) + Q_s(t)}{M_s(t) \cdot c_{p,s}(t)} \qquad (6)$$

where $T_s(t)$ and $C_{p,s}(t)$ are the average temperature and the specific heat capacity of the solution in the generator/absorber.

Inserting Eq. (1) into Eq. (4) reads:

$$\frac{dT_r(t)}{dt} = \frac{(h_v(t) - h_r(t)) \cdot \dot{m}_v(t) - Q_r(t)}{M_r(t) \cdot c_{p,r}(t)} \qquad (7)$$

where $T_r(t)$ and $C_{p,r}(t)$ are the average temperature and the specific heat capacity of the refrigerant in the condenser/evaporator. Considering the sensible heat and latent heat of the refrigerant in the refrigerant tank, the mass flow rate of refrigerant vapor can be expressed as:

$$\dot{m}_v(t) = \frac{Q_r(t) + M_r(t) \cdot c_{p,r}(t) \cdot (T_r(t) - T_r(t-1))}{h_v(t) - h_r(t)} \qquad (8)$$

3.3 Model for the overall heat transfer coefficients

Falling film heat exchangers are widely utilized in two-phase heat transfer because of high heat transfer coefficient. The heat flow in the solution component and refrigerant component is determined by the overall heat transfer coefficient and temperature difference of the heat exchanger.

$$Q = U \cdot A \cdot (\overline{T} - \overline{T}_m) \qquad (9)$$

where Q is the overall heat transfer rate. U is the overall heat transfer coefficient. A is the effective heat transfer area. $\overline{T}$ is the average temperature in each component. $\overline{T}_m$ is the logarithmic mean temperature difference of heat exchanger fluid.

The overall heat transfer coefficient U is a key parameter for analyzing absorption energy storage systems. Using average values could not accurately represent the dynamic heat transfer characteristics of

the system and introduce extra error. The thermal resistance which is the reciprocal of U, consists of the convective thermal resistance inside the tube, the thermal resistance of the tube wall and the convective thermal resistance outside the tube, expressed as:

$$\frac{1}{U} = \frac{1}{\alpha_{in}} + \frac{\delta_p}{\lambda_p} + \frac{1}{\alpha_{out}} \qquad (10)$$

where δ_p is the wall thickness of tubes, λ_p is the thermal conductivity of tubes. Because of the high thermal conductivity of the tube, the heat conduction of the tubes could be negligible. For turbulent pipe flow, the convection heat transfer coefficient inside tubes can be calculated by the Petukhov Equation [9] (Eq. (11) and (12)) as follows:

$$\alpha_{in} = \frac{Nu_{in} \bullet \lambda_f}{D_{in}} \qquad (11)$$

$$Nu = \frac{(f_m / 8) \bullet (Re - 1000) \bullet Pr}{12.7(f_m / 8)^{0.5}(Pr^{2/3} - 1) + 1} \qquad (12)$$

where λ_f is the thermal conductivity of the fluid, f_m is the Darcy friction factor expressed by Eq (13)

$$f_m = (0.79\ln(Re) - 1.64)^{-2} \qquad (13)$$

The heat transfer coefficients outside tube under different operating conditions are required to be categorized in the discussion. Therefore, different correlations are referenced from the literature [10] for the heat transfer calculations of the generator, condenser, absorber, and evaporator, respectively.

The Re number outside the pipes is governed by:

$$Re_{out} = \frac{4\Gamma}{\mu_{out}} \qquad (14)$$

The mass flow rate per unit length Γ is expressed by:

$$\Gamma = \frac{m_p}{2l} \qquad (15)$$

Heat transfer coefficient in condenser:

$$\alpha_{out} = 0.729\left[\frac{g\rho_l(\rho_l - \rho_v)k_l^3 h_{fg}}{\mu_l(T_{sat} - \overline{T}_m)D}\right]^{1/4} \qquad (16)$$

Heat transfer in evaporator:

$$\alpha_{out} = \frac{\lambda_r}{L_c} \cdot Nu_{out} \qquad (17)$$

$$Nu_{out} = 0.046Re^{0.18}Pr^{0.47} \qquad (18)$$

Heat transfer in generator:

$$\alpha_{out} = 5554.3 \cdot \Gamma^{0.236} \qquad (19)$$

Heat transfer in absorber:

$$\alpha_{out} = \frac{k_s}{\delta_s}\left(0.029\left[\frac{4 \cdot \Gamma}{\mu}\right]^{0.53}Pr_s^{0.344}\right) \qquad (20)$$

The film thickness δ_s is given by:

$$\delta_s = \left(\frac{3\mu \cdot \Gamma}{\rho^2 g} \right) \quad (21)$$

ESE and ESD are used to evaluate the performance of the energy storage system, representing the energy storage efficiency and energy storage density, respectively. The following are the calculation equations:

$$ESE = \frac{Q_a}{Q_g + W_p} \quad (22)$$

$$W_p = \frac{m_p \cdot g \cdot H}{\eta_p} \quad (23)$$

$$ESD = \frac{Q_a}{V_s + V_r} \quad (24)$$

where Q_a is the heating capacity of the absorber during the discharging. Q_e is the thermal energy input into the generator. W_p is the power consumption of the spray pump. η_p and m_p are the efficiency (80%) and mass flow rate of spray pump, respectively. H is the pump lift. V_s and V_w are the solution volume and the refrigerant volume, respectively.

3.4 Parameters settings

The heat exchangers installed in the solution tank and the refrigerant tank are designed with the same structure. The heat exchanger tube diameter is 8 mm, the heat exchange area is 0.38 m^2. The mass flow rate of the working mediums during the charging and discharging process is 0.2 kg/s. The masses of LiBr and water are 50 kg and 60 kg, respectively, and the initial concentration of the solution is 50%. To avoid crystallization of the solution during charging, the upper limit of the solution concentration is set at 65%.

Table 1 The design parameters of the absorption cycle.

Items	values	units
LiBr mass	50	kg
Refrigerant mass	60	kg
Heat exchange area	0.38	m^2
Spraying pumps	2.0	m^3/h

During the charging process, the fluid inlet temperature of the solution tank is 60 °C-90 °C, and the fluid inlet temperature of the refrigerant tank is 10 °C-30 °C. During the charging process, the fluid inlet temperature of the solution tank is 30 °C-60 °C and the fluid inlet temperature of the refrigerant tank is 10 °C-30 °C. The charging process/discharging process stops when the solution concentration in the solution tank reaches the upper limit (65%)/lower limit (55%).

4. MODEL VALIDATION

The absorption energy storage model was built in MATLAB. The thermodynamic properties of LiBr solution, including enthalpy, specific heat and vapor pressure were calculated using the fitting equation proposed by Kaita [11]. The applicable solution concentration and temperature ranges for the formulas are 40%-65% and 40 °C-210 °C, respectively. Thermophysical properties of the refrigerant, including enthalpy, specific heat, and saturated vapor pressure are also fitted from the National Institute of Standards and Technology (NIST) [12].

The measurement data from an ATS experiment [5] is used for model validation. In the initial stage of operation, the simulated solution temperature deviates from the experimental temperature because of the influence of unstable external factors. The system parameters stabilized after 20 minutes of operation, at which time the overall trends of simulated solution temperature and solution concentration are consistent with the experimental results. Compared with the experimental values, the mean square error of solution temperature and solution concentration during charging is 0.896 °C and 0.052%, respectively, while the mean square error of solution temperature and solution concentration during discharging is 0.588 °C and 0.186%, respectively.
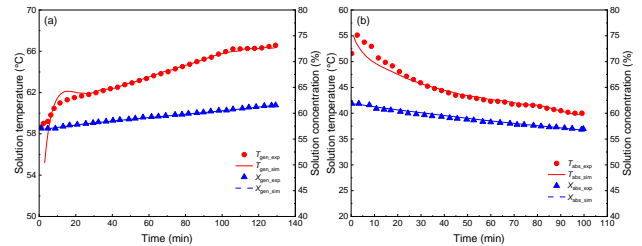

Fig.2 Model verification results (a) charging process (b) discharging process

5. RESULTS AND DISCUSSIONS

In the established model, the temperature of the external input heat source is variable, and to facilitate the analysis of the cycle performance, we keep its temperature constant. The charging and discharging temperature are the inlet water temperature during the solution charging and discharging process. To facilitate the investigation of the effects of different charge and discharge temperatures, the system was stopped after 200 minutes of operation or when the solution concentration reached the upper and lower limits.

5.1 Effects of charging temperature

Fig.3(a) shows the variation of solution concentration at different charging temperatures. The results show that the solution concentration increases with the charging temperature at the same operating time. The higher charging temperature increases the vapor pressure in the solution tank and promotes the evaporation of water from the solution tank. Fig.3(b) shows the effect of charging temperature on ESE and ESD. ESE and ESD increase with increasing charging temperature. The ESE and ESD improved by 10.4% and 62.5% as the charging temperature increased from 80 °C to 100 °C.
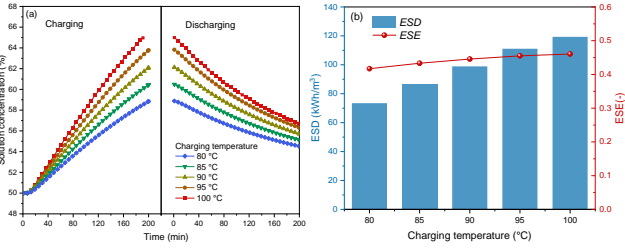
Fig.3 Effect of charging temperature on (a) solution concentration and (b) ESE and ESD.

5.2 Effects of discharging temperature

Fig.4(a) shows the variation of solution temperature and solution concentration at different discharging temperatures. The results show that the output temperature decreases rapidly for the first 20 minutes and slowly decreases until it stops during the discharging process. The output temperature increases with the increase of discharging temperature. As the discharging temperature increases, the output temperature increases and the rate of decrease of the solution concentration decreases, resulting in a decrease in the heat exchange of the absorber. Fig.4(b) shows the effect of discharging temperature on ESE and ESD. As the discharging temperature decreases from 60 °C to 40 °C, the energy storage efficiency increases from 0.25 to 0.64, while the energy storage density rises from 55.6 kWh/m^3 to 143.6 kWh/m^3.
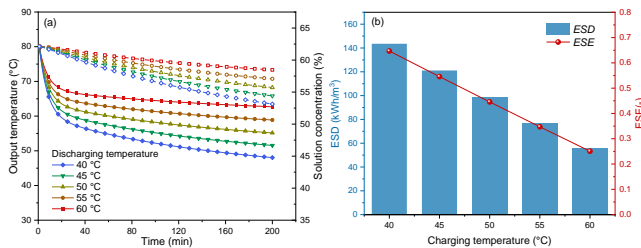

Fig.4 Effect of discharging temperature on (a) output temperature and solution concentration and (b) ESE and ESD.

5.3 Effects of operation time

To investigate the effect of condenser inlet temperature and evaporator inlet temperature on the solution energy storage characteristics, the charging process and discharging process were operated until the solution concentration reached the upper and lower limits.

Fig. 5 shows the charging time and solution temperature at the end of charging for different condenser inlet temperatures. The results show that the charging time increases significantly as the condenser inlet temperature increases. Furthermore, increasing the inlet temperature of the solution condenser is conducive to increasing the solution temperature. Fig. 6 shows the discharging time and ESE for different evaporator inlet temperatures. Discharging time and ESE are reduced by increasing the evaporator inlet temperature. This is because the higher evaporator inlet temperature increases the rate of water evaporation in the evaporator, which improves the absorber outlet temperature.
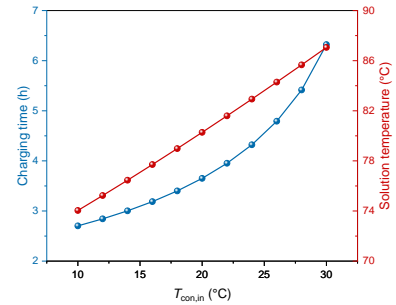

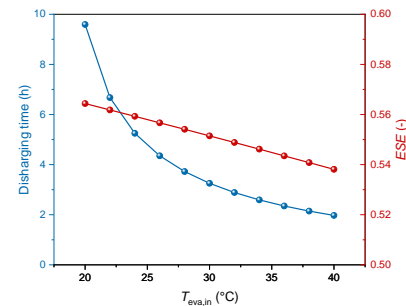*Fig.5 Charging time and solution temperature at different condenser inlet temperatures.*

Fig.6 Discharging time and ESE at different condenser inlet temperatures.

6. CONCLUSIONS

This paper proposed a novel dynamic absorption energy storage model. The dynamic model is composed of a charging process and a discharging process. The effects of charging temperature, discharging temperature, condenser inlet temperature and evaporator inlet temperature on the storage performance were investigated. The main findings can be concluded as follows:

(1) The increase in generator charging temperature promotes system storage performance. The ESE and ESD improved by 10.4% and 62.5% as the charging temperature increased from 80 °C to 100 °C.

(2) A lower discharging temperature enlarges the concentration glide and reduces output temperature. As the discharging temperature decreases from 60 °C to 40 °C, the energy storage efficiency increases from 0.25 to 0.64, while the energy storage density rises from 55.6 kWh/m^3 to 143.6 kWh/m^3, under a charging temperature of 90 °C.

(3) Lower condenser inlet temperature and higher evaporator inlet temperature resulted in a shorter charging and discharging time, respectively. The minimum charging and discharging times were 2.7 h and 1.97 h, respectively.

ACKNOWLEDGEMENT

REFERENCE

[1] Y. Zhang, R. Wang, Sorption thermal energy storage: Concept, process, applications and perspectives, Energy Storage Mater 27 (2020) 352-369.

[2] W. Cheng, B. Han, Y. Nian, B. Han, Theoretical analysis of a wind heating conversion and long distance transmission system, Energ Convers Manage 137 (2017) 21-33.

[3] N. Yu, R.Z. Wang, L.W. Wang, Sorption thermal storage for solar energy, Prog Energ Combust 39 (5) (2013) 489-514.

[4] A. Mehari, Z.Y. Xu, R.Z. Wang, Thermal energy storage using absorption cycle and system: A comprehensive review, Energ Convers Manage 206 (2020) 112482.

[5] X. Zhang, M. Li, W. Shi, B. Wang, X. Li, Experimental investigation on charging and discharging performance of absorption thermal energy storage system, Energ Convers Manage 85 (2014) 425-434.

[6] Z. Ding, W. Wu, A novel double-effect compression-assisted absorption thermal battery with high storage performance for thermal energy storage, Renew Energ 191 (2022) 902-918.

[7] M. Liu, Y. Cheng, W. Cheng, C. Zhan, Dynamic performance analysis of a solar driving absorption chiller integrated with absorption thermal energy storage, Energ Convers Manage 247 (2021) 114769.

[8] H. Wen, A. Wu, Z. Liu, Y. Shang, A State-Space Model for Dynamic Simulation of a Single-Effect LiBr/H2O Absorption Chiller, Ieee Access 7 (2019) 57251-57258.

[9] Z. Deng, Y. Nian, W. Cheng, Estimation method of layered ground thermal conductivity for U-tube BHE based on the quasi-3D model, Renew Energ 213 (2023) 121-133.

[10] A.A.V. Ochoa, J.C.C. Dutra, J.R.G. Henríquez, C.A.C. Dos Santos, J. Rohatgi, The influence of the overall heat transfer coefficients in the dynamic behavior of a single effect absorption chiller using the pair LiBr/H2O, Energ Convers Manage 136 (2017) 270-282.

[11] Y. Kaita, Thermodynamic properties of lithium bromide–water solutions at high temperatures, Int J Refrig 24 (5) (2001) 374-390.

[12] E.W. Lemmon, M.L. Huber, M.O. McLinden, NIST Standard Reference Database 23:eference Fluid Thermodynamic and Transport Properties-REFPROP, Version 9.1 | NIST, in, 2013.